Normalized Nonlinear Impedance Boundary Condition in Anhysteretic Magnetic Material for Eddy Current Problems

Claudio Carretero[1], *Senior Member, IEEE*, Jesus Acero[2], *Senior Member, IEEE*, and Jose M. Burdio[2], *Senior Member, IEEE*
[1]Dept. Applied Physics. University of Zaragoza. 50009 Zaragoza (Spain).
[2]Dept. Electronic Engineering and Communications. University of Zaragoza. 50018 Zaragoza (Spain).

Numerical simulations of induction heating systems often assume that the properties of the induction load are linear. Thus, its electrical behavior is described by an equivalent impedance which exhibits frequency dispersion but remains independent of the excitation level. Although deriving such solutions is computationally complex, the use of the impedance boundary condition (IBC) provides high-quality results for linear media. This boundary condition replaces the effects of media with rapidly varying fields by a ratio between their tangential components at the surface. However, in typical induction loads, magnetic saturation of the material causes phenomena of dependence of the properties on the current level. The precise formulation of such an IBC can only be performed considering linear media. This paper proposes calculating a nonlinear excitation level-dependent IBC numerically, considering the saturation dependence of the magnetic properties given by a Langevin function BH-loop. A normalized form of the nonlinear IBC will be obtained from the equation governing this type of behavior, thereby reducing the computational cost of the solution. The usefulness of the proposed nonlinear IBC will be validated by comparing it with results obtained from conventional time domain simulations of a typical induction heating system.

***Index Terms*—Eddy currents, induction heating, home appliances, impedance boundary condition.**

I. Introduction

EDDY currents are a common phenomenon encountered in various problems. Induction heating (IH) is a particularly significant application of eddy currents, owing to its widespread utilization in multiple technological domains. However, efficient numerical solutions for eddy current problems pose significant challenges due to the complex behavior of electromagnetic fields, which feature a combination of smooth spatial variations and abrupt changes. Some analytical solutions for simple geometries of this kind of problems can be found in the literature, mainly for layered structures with axial symmetry [1], [2], [3], or structures with cylindrical symmetry [4], [5], [6], [7], [8]. However, the extension of the treatment to more complex geometries requires the application of numerical methods which involve high computational cost [9], [10]. The application of numerical methods for the resolution of eddy current systems has been an active field of work in the past, as can be found in [11] to obtain an optimized pattern of power dissipated in a metallic element, in [12] for cold crucible melting processes, in [13] for the numerical simulation of hardening by induction heating, in [14] for domestic induction heating, in [15], [16] coupling electro-thermal effects and in [17] for coupled electro-thermal automated induction heating treatment of surfaces.

In an attempt to simplify the calculation process with an acceptable reduction in accuracy, the use of the so-called impedance boundary condition (IBC), which replaces the penetration of electromagnetic fields into a conductive material with a Robin boundary condition, is appropriate. The definition of the most suitable IBCs for electromagnetic problems has been extensively studied for applications in the frequency domain, both in the high-frequency regime, where systems correspond to electromagnetic wave scattering problems [18], and in the quasi-static regime [19], [20], [21].

In general, the level of the electromagnetic fields is sufficiently reduced to ensure the material properties are independent of the excitation value. However, particularly in induction heating applications, the fields at the material boundary often reach high values and can magnetically saturate the material. In this case, it is observed that the material properties depend on the applied excitation, therefore the solutions in the frequency domain are not totally correct because they are derived based on the superposition principle. Some alternatives have been proposed by various authors to include the nonlinear magnetic properties in eddy current systems. In [22], the problem is divided into two coupled methods: a 1-D approach for handling the nonlinearity and a 3-D approach that works on the aligned problem, although it has the disadvantage of requiring a high computational cost and obtaining a rather limited accuracy in the results. Achieving accurate results is determined by an adequate characterization of the magnetic properties of the material [23]. The number of proposals inferring the expression of the impedance boundary condition for nonlinear magnetic material is remarkable because this approach presents great advantages in the calculation of approximate numerical solutions. The BH-loop describes the magnetic characteristics of the material and constitutes the starting point for any nonlinear impedance boundary approach. The impedance boundary condition for the case of extreme saturation with a step dependence of the BH-loop is provided in [24], [25], [26] based on the analytical solution of the field diffusion inside the material. An alternative expression for the IBC of a nonlinear magnetic infinite half-space is also derived in [27] based on the fitting of the BH-loop.

Manuscript received December 21, 2023; revised February 28, 2024 and April 7, 2024; accepted April 22, 2024. Corresponding author: C. Carretero (email: ccar@unizar.es).

Several authors have proposed to solve the 1-D equation by numerical methods to obtain the nonlinear IBC under different functional dependencies of the BH-loop curve. In reference to BH-loops, various techniques have been proposed for dealing with the nonlinear IBC. For instance, the finite difference method based on the Frohlich-Kennelly relation is explained in [28]. Additionally, a finite integration technique extraction is provided in [29], whereas [30] proposes a finite element method calculation that also considers the temperature dependence of the material's electrical conductivity. Alternatively, some hybrid methods have been proposed that combine the linear boundary impedance condition and the boundary impedance condition for step-like dependence using some weighting methods, as given in [31], [32], or for fitting methods performed from the application of the finite difference method [33].

The application of nonlinear IBC has been reported in several recent works to reduce the computational cost in the finite element method [34] and the boundary element method [35], [36].

The design of IH systems is carried out by numerical simulation of complex 3D geometries to capture the complexity of their structure using commercial tool models. In these models, the IBC is applied to reduce the computational costs of the simulation. The nonlinear behavior of the load is not well established and is sometimes modeled by an equivalent complex relative permeability calculated from a mean field approach, [37]. However, results are accurate for conditions prevailing at operating frequencies and field levels to deliver maximum power to the load, but inaccuracies appear at different operational points. The objective of this work is to propose a normalized nonlinear IBC in this hybrid regime for the Langevin function BH-loop by applying numerical methods.

The remainder of the paper is organized as follows: Section II presents some basics on the modeling of IBC. In Section III are described the main results to calculate the nonlinear IBC for the proposed Langevin function BH-loop and the derivation of the normalized form of the nonlinear IBC. Section IV is dedicated to the practical application of the proposed form for the nonlinear boundary condition to a reference system of a typical induction heating system under different conditions. Finally, some conclusion are drawn in the last section of the paper.

II. Impedance Boundary Condition

Regarding the numerical analysis of eddy current problems, the IBC reduces the complexity and computational cost of the harmonic solution. In this approach, the sharply varying fields near the surface of the conductors are substituted by the following relationship in the surface [38]:

$$\hat{\mathbf{n}} \times \mathbf{E}_0 = Z_{\mathrm{L}} \left(\hat{\mathbf{n}} \times \mathbf{H}_0 \right) \times \hat{\mathbf{n}}, \tag{1}$$

where $\hat{\mathbf{n}}$ is the normal vector pointing outward the conductor material, $\mathbf{E}_0$ and $\mathbf{H}_0$ are the electric field complex amplitude and the magnetic field complex amplitude at angular frequency ω, respectively, and Z_{L} is the surface impedance for linear materials at angular frequency ω.

The IBC modeling requires solving a simple numerical 1-dimensional equation. The governing equations of the electromagnetic fields correspond to the time-dependent Maxwell's equations. Applying some manipulations to the preceding equations for a transverse magnetic field plane-wave incident to a magnetic and conductive half space beyond $z = 0$, they can be reduced to the basic single expression [39]:

$$\frac{\partial h}{\partial t} = \frac{1}{\mu\sigma} \frac{\partial^2 h}{\partial z^2}. \tag{2}$$

where $h\left(t\right) = H_0 \sin\left(\omega t\right)$ is the time-dependent transverse magnetic field, σ and μ are the conductivity and permeability of the material, respectively.

Solving the preceding equation, the well-known expression of the IBC for a linear material can be obtained:

$$Z_{\mathrm{L}} = \sqrt{\frac{\omega\mu}{\sigma}} e^{i\frac{\pi}{4}} = \frac{1+i}{\sigma\delta}, \tag{3}$$

where δ is the penetration depth.

The IBC presents a precise solution to eddy current problems within the medium frequency range of several hundred of hertz to megahertz. In that case, the fields can be described by diffusion equations and radiation terms can be neglected without loss of generality. However, although the IBC approach is suitable for solving a wide variety of eddy current systems including conducting material, it gives inaccurate results for material with nonlinear magnetic properties. In the past, many works have focused on nonlinear behavior using a variety of approaches. The first successful analytical description of a nonlinearity in the magnetic properties of a material is given by Agarwal in its celebrated work [25], for a step-like BH-loop, giving the impedance boundary condition by:

$$Z_{\mathrm{sat}} = 1.34 e^{-0.102\pi i} Z_{\mathrm{L}} \left(\mu_{\mathrm{m}}\right). \tag{4}$$

where $\mu_{\mathrm{m}} = B_{\mathrm{sat}}/H_0$ is the equivalent magnetic permeability for a saturable material and $Z_{\mathrm{L}}\left(\mu_{\mathrm{m}}\right)$ is the expression of the linear IBC substituting the linear magnetic permeability by the equivalent magnetic permeability for a saturable material.

III. Nonlinear impedance boundary condition from finite difference method

A. Langevin function anhysteretic BH-loop

Magnetic properties of soft materials can be described by the Langevin function, which is used to define anhysteretic magnetization in the Jiles-Atherton model, as it is presented as follows [40]:

$$M_{\mathrm{an}}\left(H\right) = M_{\mathrm{sat}} \left(\coth\left(\frac{H}{a}\right) - \frac{1}{H/a} \right), \tag{5}$$

where M_{sat} is the saturation magnetization, the domain wall parameter a is the factor governing the slope of the curve and H is the magnetic field. The magnetic flux field is given by the identity $B = \mu_0 M_{\mathrm{an}}\left(H\right) + \mu_0 H$, and the saturation B-field is therefore defined as $B_{\mathrm{sat}} = \mu_0 M_{\mathrm{sat}}$.

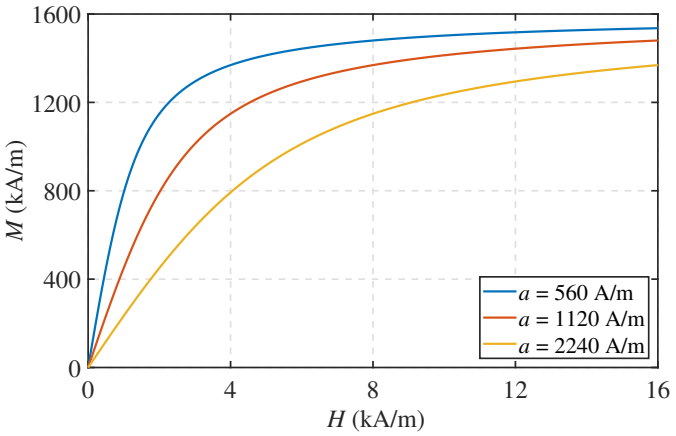

Fig. 1: Langevin function BH-loop for $B_{\text{sat}} = 2$ T at different domain wall parameter a.

The differential relative permeability can be obtained by applying the derivative of the magnetic flux field with respect to the magnetic field $\mu_{\text{r,diff}} = \frac{1}{\mu_0} dB/dH$, then, we have:

$$\mu_{\text{r,diff}}(H) = \frac{B_{\text{sat}}}{a\mu_0}\left(1 - \coth^2\left(\frac{H}{a}\right) - \frac{1}{(H/a)^2}\right) + 1. \quad (6)$$

The dependence of the magnetization field and differential relative permeability for a material with the typical saturation of magnetic steel, $B_{\text{sat}} = 2$ T, and electrical conductivity $\sigma = 1.12 \cdot 10^7$ S/m is shown in Figure 1. As can be seen, the domain wall parameter a governs the dependence on these parameters by resizing the different curves, in particular, the maximum level is given as an initial permeability:

$$\mu_{\text{r,ini}} = \frac{B_{\text{sat}}}{3a\mu_0} + 1 \approx \frac{M_{\text{sat}}}{3a\mu_0}. \quad (7)$$

Therefore, considering the relationship $a = \frac{B_{\text{sat}}}{3(\mu_{\text{r,ini}}-1)\mu_0}$, equation (6) can be rewritten as:

$$\mu_{\text{r,diff}}(H) = 3(\mu_{\text{r,ini}} - 1)\cdot\left(1 - \coth^2\left(\frac{H}{a}\right) - \frac{1}{(H/a)^2}\right) + 1. \quad (8)$$

Considering the field dependence as $F(H/a) = \left(1 - \coth^2\left(\frac{H}{a}\right) - \frac{1}{(H/a)^2}\right)$, we have:

$$\mu_{\text{r,diff}}(H) = 3(\mu_{\text{r,ini}} - 1) F(H/a) + 1. \quad (9)$$

The impact of hysteresis is not taken into account in this analysis because it increases complexity with reduced additional explanatory power when dealing with soft materials, as is often the case in eddy current problems.

B. Finite difference method applied to diffusion field equation

The finite difference method constitutes a good choice to obtain the IBC of a nonlinear material due to its efficiency and ease of implementation in general-purpose programming languages. In this particular case, MATLAB®has been chosen because facilitates the programming of the code for this application. An implicit definition of the finite difference method is selected because an unconditional stable algorithm can avoid any additional problems in the simulation.

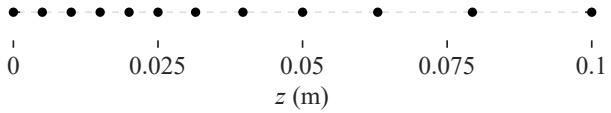

Fig. 2: Unstructured 1-D mesh composed of an evenly spaced grid at low z-coordinates and increasing spacing at higher z-coordinates.

As it was previously mentioned, impedance boundary modeling requires a simple numerical 1-dimensional simulation based on time-dependent Maxwell's equations. Rearranging the preceding equations under the conditions exhibited in nonlinear eddy current problems, it can be obtained the basic single expression [39]:

$$\frac{\partial h}{\partial t} = \frac{\frac{\partial^2 h}{\partial z^2}}{\mu_0\sigma\left(1 + \frac{\partial M}{\partial h}\right)}. \quad (10)$$

where M is the magnetization at the magnetic field level $h(t)$ and μ_0 is the vacuum permeability. Alternatively, the preceding expression can be rewritten including the definition of relative differential permeability, as shown as follows:

$$\frac{\partial h}{\partial t} = \frac{\frac{\partial^2 h}{\partial z^2}}{\mu_0\sigma\mu_{\text{r,diff}}(h)}. \quad (11)$$

The preceding expression can be easily solved by the finite difference method for the harmonic excitation at $z = 0$ of the form $h(t) = H_0 \sin(\omega t)$, and assuming vanishing fields at $z \to \infty$. In the case under study, a discretization for an unstructured mesh is applied because a finer sampling is considered for the rapidly varying fields near to $z = 0$ and a coarser mesh is applied at a higher z position where the field tends to be almost zero, as can be seen in Figure 2

The spatial derivative of the magnetic field can be derived from the Taylor's expansion:

$$\left.\frac{\partial^2 h}{\partial z^2}\right|_i^n = \frac{2\Delta z_i^{\text{L}}}{D_i^{\text{LR}}} h_{i-1}^n + \frac{2\left(\Delta z_i^{\text{L}} + \Delta z_i^{\text{R}}\right)}{D_i^{\text{LR}}} h_i^n + \frac{2\Delta z_i^{\text{R}}}{D_i^{\text{LR}}} h_{i+1}^n, \quad (12)$$

where superscript n represent the time sampling number, subscript i represent the z-coordinate sampling number, $\Delta z_i^{\text{R}} = z_{i+1} - z_i$ and $\Delta z_i^{\text{L}} = z_i - z_{i-1}$ are the upward and downward sampling distances, respectively, and $D_i^{\text{LR}} = \Delta z_i^{\text{L}}\left(\Delta z_i^{\text{R}}\right)^2 + \left(\Delta z_i^{\text{L}}\right)^2 \Delta z_i^{\text{R}}$ normalizes the expression.

Time discretization is performed in a standard manner as follows:

$$\left.\frac{\partial h}{\partial t}\right|_i^n = \frac{h_i^{n+1} - h_i^n}{\Delta t}, \quad (13)$$

where Δt is the increase of time selected for the discretization.

The discretization of equation (11) can be achieved using an explicit algorithm where the spatial derivative is evaluated at instant n. However, this approach may result in unstable output values despite being computationally efficient. To improve the stability of the solution, an implicit type algorithm will be used to estimate the spatial derivative at the $n+1$ instant. Additionally, to avoid the use of iterative solution algorithms, the value of the relative magnetic permeability, $\mu_{\mathrm{r,diff}}$, will be calculated at instant n. Therefore, equation (11) can be expressed as:

$$\left.\frac{\partial h}{\partial t}\right|_i^n = \frac{1}{\mu_0 \sigma \mu_{\mathrm{r,diff}}\left(h_i^n\right)} \left.\frac{\partial^2 h}{\partial z^2}\right|_i^{n+1}. \tag{14}$$

Substituting (12) and (13) into (14), we obtain:

$$\frac{h_i^{n+1}-h_i^n}{\Delta t} = \frac{1}{\mu_0 \sigma \mu_{\mathrm{r,diff}}\left(h_i^n\right)} \cdot \left[\frac{2\Delta z_i^{\mathrm{L}}}{D_i^{\mathrm{LR}}} h_{i-1}^{n+1} + \frac{2\left(\Delta z_i^{\mathrm{L}}+\Delta z_i^{\mathrm{R}}\right)}{D_i^{\mathrm{LR}}} h_i^{n+1} + \frac{2\Delta z_i^{\mathrm{R}}}{D_i^{\mathrm{LR}}} h_{i+1}^{n+1}\right]. \tag{15}$$

Rearranging the expression, we have:

$$h_i^n = h_i^{n+1} - \frac{\Delta t}{\mu_0 \sigma \mu_{\mathrm{r,diff}}\left(h_i^n\right)} \cdot \left[\frac{2\Delta z_i^{\mathrm{L}}}{D_i^{\mathrm{LR}}} h_{i-1}^{n+1} + \frac{2\left(\Delta z_i^{\mathrm{L}}+\Delta z_i^{\mathrm{R}}\right)}{D_i^{\mathrm{LR}}} h_i^{n+1} + \frac{2\Delta z_i^{\mathrm{R}}}{D_i^{\mathrm{LR}}} h_{i+1}^{n+1}\right]. \tag{16}$$

The preceding relationship establishes a system of equations to be solved. By defining the column vector $\overline{h}^n = \left[h_1^n \cdots h_i^n \cdots h_{n_s}^n\right]^{\mathrm{T}}$, it can be expressed as:

$$\overline{\overline{B}}^n \cdot \overline{h}^{n+1} = \overline{h}^n. \tag{17}$$

where $\overline{\overline{B}}^n$ is a matrix of elements b_{ij}^n.

The upper-diagonal elements $b_{i(i+1)}^n$ are defined as:

$$b_{i(i+1)}^n = -\frac{2\Delta z_i^{\mathrm{R}} \Delta t}{\mu_0 \sigma \mu_{\mathrm{r,diff}}\left(h_i^n\right) D_i^{\mathrm{LR}}}, \tag{18}$$

the diagonal elements b_{ii}^n are defined as:

$$b_{ii}^n = 1 - \frac{2\left(\Delta z_i^{\mathrm{L}} + \Delta z_i^{\mathrm{R}}\right)\Delta t}{\mu_0 \sigma \mu_{\mathrm{r,diff}}\left(h_i^n\right) D_i^{\mathrm{LR}}}, \tag{19}$$

the lower-diagonal elements $b_{i(i-1)}^n$ are defined as:

$$b_{i(i-1)}^n = -\frac{2\Delta z_i^{\mathrm{L}} \Delta t}{\mu_0 \sigma \mu_{\mathrm{r,diff}}\left(h_i^n\right) D_i^{\mathrm{LR}}}, \tag{20}$$

otherwise, if. $j' \neq i-1$, $j' \neq i$ and $j' \neq i-1$, then $b_{ij'} = 0$. $\overline{\overline{B}}^n$ is a tridiagonal matrix with non-zero values only on the main diagonal and the diagonals immediately above and below it:

$$\overline{\overline{B}}^n = \begin{bmatrix} b_{11}^n & b_{12}^n & 0 & & 0 & 0 & 0 & & 0 & 0 & 0 \\ b_{21}^n & b_{22}^n & b_{23}^n & \cdots & 0 & 0 & 0 & & 0 & 0 & 0 \\ 0 & b_{32}^n & b_{33}^n & & 0 & 0 & 0 & & 0 & 0 & 0 \\ & \vdots & & \ddots & & \vdots & & \iddots & & \vdots & \\ 0 & 0 & 0 & & b_{(i-1)(i-1)}^n & b_{(i-1)i}^n & 0 & & 0 & 0 & 0 \\ 0 & 0 & 0 & \cdots & b_{i(i-1)}^n & b_{ii}^n & b_{i(i+1)}^n & \cdots & 0 & 0 & 0 \\ 0 & 0 & 0 & & 0 & b_{(i+1)i}^n & b_{(i+1)(i+1)}^n & & 0 & 0 & 0 \\ & \vdots & & \iddots & & \vdots & & \ddots & & \vdots & \\ 0 & 0 & 0 & & 0 & 0 & 0 & & b_{(n_s-2)(n_s-2)}^n & b_{(n_s-2)(n_s-1)}^n & 0 \\ 0 & 0 & 0 & \cdots & 0 & 0 & 0 & \cdots & b_{(n_s-1)(n_s-2)}^n & b_{(n_s-1)(n_s-1)}^n & b_{n_s(n_s-1)}^n \\ 0 & 0 & 0 & & 0 & 0 & 0 & & 0 & b_{n_s(n_s-1)}^n & b_{n_s n_s}^n \end{bmatrix} \tag{21}$$

The calculation of the next-step magnetic field $\overline{h}^{n+1}$ can be obtained by applying:

$$\overline{h}^{n+1} = \left(\overline{\overline{B}}^n\right)^{-1} \cdot \overline{h}^n. \tag{22}$$

Obviously, the inversion of the matrix $\overline{\overline{B}}^n$ is responsible for the majority of the procedure's computational cost.

C. Nonlinear impedance boundary from FDM results

The boundary conditions to be applied to obtain the transient solution of the magnetic field in the material are listed as follows: the magnetic field at the boundary between the media, the value of the magnetic field at the initial instant and the magnetic field at the latter spatial point.

In the first case, the excitation to be applied is a discretized harmonic type signal at $t^n = (n-1)\Delta t$. Therefore, the condition at the boundary is:

$$h_1^n = H_0 \cdot \sin\left(2\pi f\left(n-1\right)t\right) \quad \text{where } n \in [0, N]. \tag{23}$$

where the spatial subscripts indicate the position $z = 0$.

The initial value of the field inside the magnetic medium can be set to zero, or to a different value derived from a previous simulation. Null values imply a larger simulation to reach steady-state configuration, but it constitutes the simplest constraint to start the procedure, as it is given as follows:

$$h_i^1 = 0 \quad \text{where } i \in [0, n_{\mathrm{s}}]. \tag{24}$$

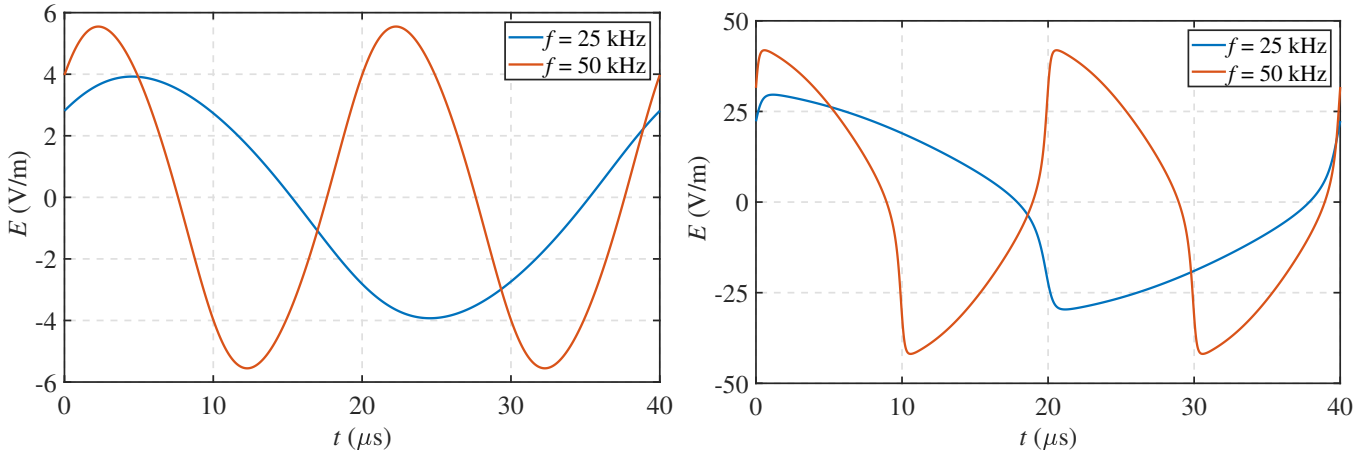

(a) $H_0 = 1000$ A/m. (b) $H_0 = 16000$ A/m.

Fig. 3: Electric field at the boundary of a magnetic anhysteretic material of conductivity $\sigma = 1.12 \cdot 10^7$ S/m, $B_{\text{sat}} = 2$ T and $a = 560$ A/m , at two different excitation frequencies for equal magnetic field amplitude at the boundary.

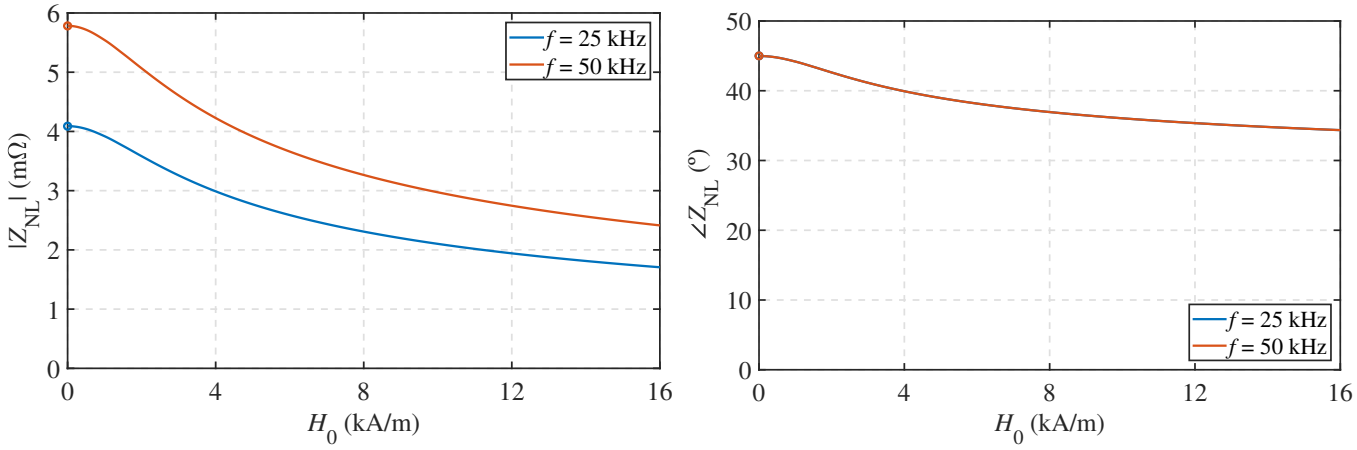

(a) IBC amplitude. (b) IBC phase.

Fig. 4: First harmonic IBC dependence with respect to the magnetic field amplitude for a material with $\sigma = 1.12 \cdot 10^7$ S/m, $B_{\text{sat}} = 2$ T and $a = 560$ A/m (continuous line), and linear IBC for the initial magnetic permeability (circular symbols), at different excitation frequencies.

The magnetic field vanishes at larger distances from the boundary of the magnetic medium, $\lim_{z\to\infty} h(z,t) \to 0$, thus:

$$h_{n_s}^n = 0 \quad \text{where } n \in [0, N]\,. \tag{25}$$

Starting by (23), expression (22) is iteratively applied to obtain $\overline{h}^{(n+1)}$, but elements $h_1^{(n+1)}$ and $h_{n_s}^n$ would be substituted by applying (23) and (25), respectively.

The accuracy of the results depends on the discretization conditions. As it was mentioned, the proposed algorithm admits non-uniform spatial sampling. The first samples are equally spaced, due to the linear decay of the magnetic field when the material is in deep saturation. In the remaining ones, corresponding to greater depths in the material, an exponential spacing has been applied, because the field presents this dependence.

IBC extraction implies a relationship between the electric field and magnetic field complex amplitudes at the boundary position. The time-domain tangential electric field is related to the tangential magnetic field by considering its relationship with the electrical current in a conductive media and the Ampere's law establishing, thus:

$$e\,(t, z=0) = \frac{1}{\sigma}\frac{\partial h}{\partial z}\bigg|_{z=0}. \tag{26}$$

An accurate numerical derivative is obtained by using a multiple-sample value scheme, which requires a uniform sampling Δz in the first samples, as it is given as follows:

$$\frac{\partial h}{\partial z}\bigg|_{z=0}^{n} = \frac{-3h_1^n + 4h_2^n - h_3^n}{2\Delta z}, \tag{27}$$

where h_1^n, h_2^n and h_3^n are the solutions for the magnetic fields at the boundary position $z_1 = 0$, position $z_2 = \Delta z$ and position $z_3 = 2\Delta z$, respectively. Higher order formulation can be considered but less precision can be achieved due to the

nonlinear spatial variation of the fields. By combining both equations, we have:

$$e\left(t, z=0\right) = \frac{-3h_1^n + 4h_2^n - h_3^n}{2\sigma\Delta z}, \tag{28}$$

Finer meshing close to the transition boundary at $z \approx 0$ contributes to a precise numerical calculation of the electric component because fields exhibit a rapid decay inside the conductive medium.

Steady-state electric fields are represented in Figure 3(a) for the linear regime and in Figure 3(b) for the highly saturation regime, respectively. At the magnetic amplitude level of 1000 A/m, the time dependence of the electric field is almost a sinusoidal signal for both excitation frequencies due to the maximum level does not reach the saturation of the material. However, at large signal levels, as shown in Figure 3(b), the waveform of the electric field becomes distorted due to saturation of the material. It tends to the Agarwal model for extreme magnetic saturation.

The harmonic extraction of the steady-state signal is required to calculate the IBC at the ratio between the electric field and the magnetic field at $z = 0$. The harmonic n_h of the transverse magnetic field is defined as:

$$\hat{H}\left(n_h\right) = \frac{\omega}{2\pi}\int_0^{\frac{2\pi}{\omega}} h\left(t\right) e^{j\omega n_h t} dt. \tag{29}$$

In this approach, the nonlinear IBC $Z_{\mathrm{NL}}\left(H_0\right)$ is derived from the first harmonic of the transverse magnetic field amplitude $\hat{H}\left(1\right)$:

$$Z_{\mathrm{NL}}\left(H_0\right) = \left.\frac{\frac{\partial \hat{H}(1)}{\partial z}}{\sigma \hat{H}\left(1\right)}\right|_{z=0}. \tag{30}$$

The first harmonic IBC $Z_{\mathrm{NL}}\left(H_0\right)$ depends on the peak level of the magnetic field applied at the transition media H_0, as shown in Figure 4. The magnitude of the IBC decreases at higher field level, whereas, the phase of the complex value of the impedance boundary condition also reduces. However, the primary conclusion drawn from Figure 4 is about the self-similarity of the IBC dependencies concerning frequency. The magnitudes appear to be proportional between them at different frequencies, and the phase seems to be independent of the excitation frequencies.

D. Normalized form of nonlinear impedance boundary condition

The nonlinear IBC for a material whose magnetization curve obeys the anhysteretic Langevin function BH-loop can be normalized by taking advantages of the mathematical characteristics of the aforementioned differential equation (11).

Normalization to the frequency f_0 can be performed by rescaling time variable $t' = \left(f/f_0\right)t$ in the excitation applied at $z = 0$:

$$h'\left(t'\right) = H_0' \sin\left(2\pi f_0 t'\right). \tag{31}$$

Therefore, the left-hand side of (11) becomes:

$$\frac{\partial h}{\partial t} = \frac{\partial h'}{\partial t'}\frac{\partial t'}{\partial t} = \frac{f}{f_0}\frac{\partial h'}{\partial t'}, \tag{32}$$

Due to the properties of the anhysteretic magnetization curve, the differential permeability possesses an approximated self-similarity dependence on the saturation magnetic flux field $B_{\mathrm{sat}} = \mu_0 M_{\mathrm{sat}}$ and domain wall density a, as it can be derived from (7):

$$\mu_{\mathrm{r,diff}}\left(B_{\mathrm{sat}}, a, h\right) = \frac{B_{\mathrm{sat}}}{3a\mu_0} F\left\{\frac{h}{a}\right\} + 1, \tag{33}$$

but maybe approximated by:

$$\mu_{\mathrm{r,diff}}\left(B_{\mathrm{sat}}, a, h\right) \approx \frac{B_{\mathrm{sat}}}{3a\mu_0} F\left\{\frac{h}{a}\right\}. \tag{34}$$

Applying the substitution $h/a = h'/a_0$, i.e., $H_0/a = H_0'/a_0$ because the time dependence is the same at $z = 0$, and therefore, the excitation amplitude obeys:

$$H_0 = \frac{a}{a_0} {H'}_0. \tag{35}$$

Then, equation (34) can be rearranged as follows:

$$\mu_{\mathrm{r,diff}}\left(B_{\mathrm{sat}}, a, h\right) \approx \frac{B_{\mathrm{sat}}}{B_{\mathrm{sat},0}}\frac{a_0}{a}\frac{B_{\mathrm{sat},0}}{3a_0\mu_0} F\left\{\frac{h'}{a_0}\right\}. \tag{36}$$

Therefore:

$$\mu_{\mathrm{r,diff}}\left(B_{\mathrm{sat}}, a, h\right) \approx \frac{B_{\mathrm{sat}}}{B_{\mathrm{sat},0}}\frac{a_0}{a}\mu_{\mathrm{r,diff}}\left(B_{\mathrm{sat},0}, a_0, h'\right). \tag{37}$$

Substituting (37) and (32) into equation (11):

$$\frac{\partial h'}{\partial t'} = \left(\frac{f_0}{f}\frac{\sigma_0}{\sigma}\frac{B_{\mathrm{sat},0}}{B_{\mathrm{sat}}}\frac{a}{a_0}\right)\frac{\frac{\partial^2 h'}{\partial z^2}}{\mu_0\sigma_0\mu_{\mathrm{r,diff}}\left(B_{\mathrm{sat},0}, a_0, h'\right)}. \tag{38}$$

Normalizing the spatial variable z' as follows:

$$z' = z\sqrt{\frac{f}{f_0}\frac{\sigma}{\sigma_0}\frac{B_{\mathrm{sat}}}{B_{\mathrm{sat},0}}\frac{a_0}{a}}. \tag{39}$$

The equation (37) is transformed into its normalized version:

$$\frac{\partial h'}{\partial t'} = \frac{\frac{\partial^2 h'}{\partial z'^2}}{\mu_0\sigma_0\mu_{\mathrm{r,diff}}\left(B_{\mathrm{sat},0}, a_0, h'\right)}. \tag{40}$$

The nonlinear boundary impedance condition from the solution of the above equation can be obtained by rearranging (30) in the following form:

$$Z_{\mathrm{NL}}\left(H_0\right) = \frac{\sigma_0}{\sigma}\frac{\partial z'}{\partial z}\left.\frac{\frac{\partial \hat{H}'(1)}{\partial z'}}{\sigma_0 \hat{H}'\left(1\right)}\right|_{z=0} = \frac{\sigma_0}{\sigma}\frac{\partial z'}{\partial z} Z'_{\mathrm{NL}}\left(H_0'\right). \tag{41}$$

Applying the substitutions provided in (35) and (39), we obtain:

$$Z_{\mathrm{NL}}\left(H_0\right) = \sqrt{\frac{f}{f_0}\frac{\sigma_0}{\sigma}\frac{B_{\mathrm{sat}}}{B_{\mathrm{sat},0}}\frac{a_0}{a}} Z'_{\mathrm{NL}}\left(H_0\frac{a_0}{a}\right). \tag{42}$$

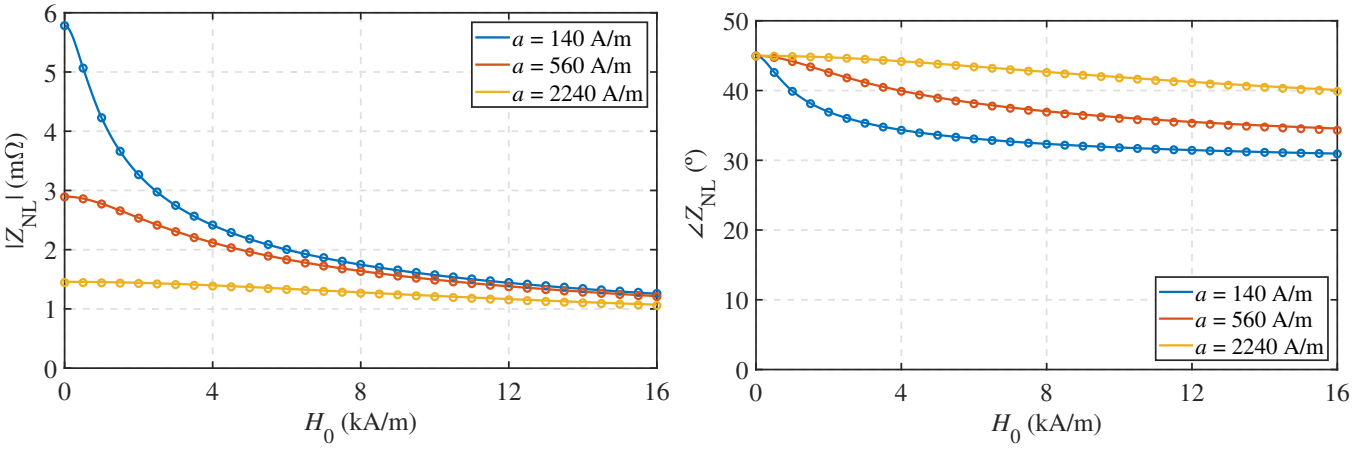

(a) IBC amplitude. (b) IBC phase.

Fig. 5: Comparison between the IBC dependence with respect to the magnetic field amplitude for a material with $\sigma = 1.12 \cdot 10^7$ S/m, $f = 50$ kHz and $B_{\text{sat}} = 0.5$ T, at different domain wall parameter a (continuous lines) and the derived values from the scaled normalized impedance (circular symbols).

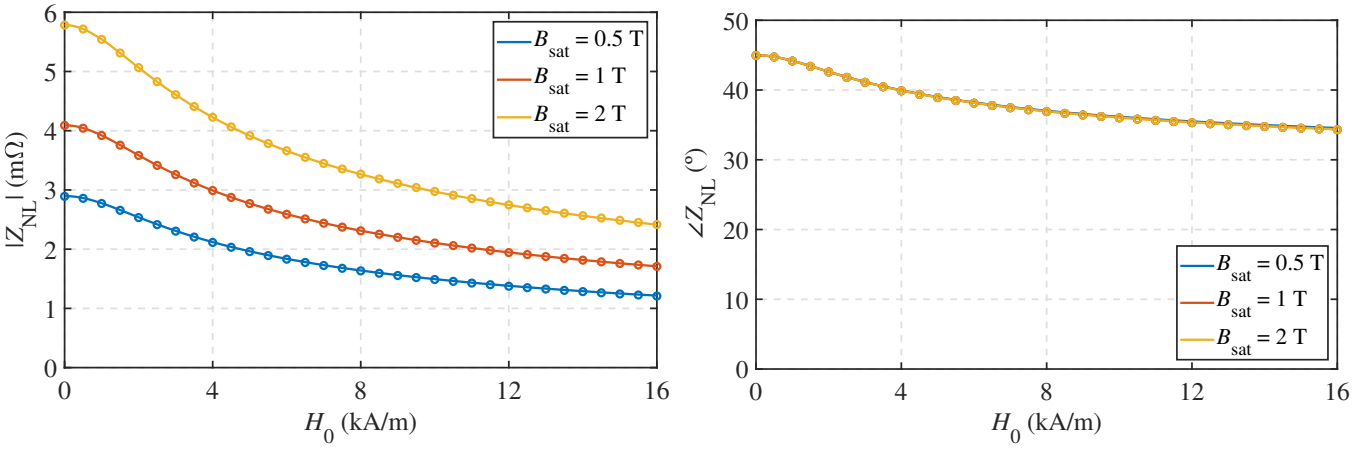

(a) IBC amplitude. (b) IBC phase.

Fig. 6: Comparison between the IBC dependence with respect to the magnetic field amplitude for a material with $\sigma = 1.12 \cdot 10^7$ S/m, $f = 50$ kHz, and domain wall parameter $a = 560$ A/m, at different magnetic saturation values B_{sat} (continuous lines) and the derived values from the scaled normalized impedance (circular symbols).

where $Z'_{\text{NL}}(H'_0)$ is the normalized nonlinear boundary impendence condition. Expression (42) is not exact due to the approximation taken from (33) to (34), but gives accurate results if the initial permeability of the BH-loop is higher than μ_0.

Figure 5 shows the comparison between the impedance boundary condition absolute values and phases with respect to the field level amplitude at different domain wall parameters a obtained from a numerical calculation and the derived value given by the equation (42), for the reference IBC $Z'_{\text{NL}}(H'_0)$ at $f_0 = 10$ kHz, $\sigma_0 = 1.12 \cdot 10^7$ S/m and $B_{\text{sat},0} = 2$ T. As it can be seen in Figure 5(a), the accuracy of the derived absolute values is good at the different excitation magnetic field level under analysis, whereas the phase of the impedance boundary condition remains invariant with respect to the field level, as it is shown in Figure 5(b). In this case, the change in the parameter a also implies escalating the excitation magnetic field amplitude, thus, the range derived from the reference IBC $Z_{\text{NL},0}(H_0)$ is proportional to the relationship between the domain wall parameter a and the reference value $a_0 = 560$ A/m.

In addition, the comparison of the IBC values between calculated data and the derived from (42) for different magnetic saturation values B_{sat} are represented in Figure 6, where the good agreement between the values derived from $Z'_{\text{NL}}(H'_0)$ and the simulation results for the whole set of parameters is evident.

IV. Practical Application of the Impedance Boundary Condition

The IBC is extensively employed in the numerical simulation of electromagnetic systems which involve conductive and magnetic components in the quasi-static regime. For

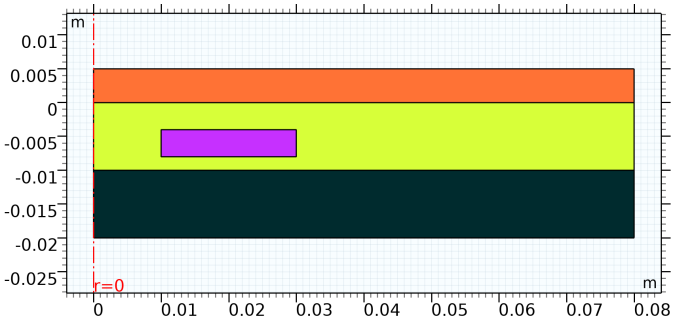

Fig. 7: 2D-axisymmetric model of IH system with nonlinear load.

illustrative purposes, the usefulness of the nonlinear IBC will be demonstrated for a simple induction heating system structure composed of a spiral coil placed between two half-space media. This structure captures, in a general form, the behavior of an induction cooker whose load operates at the boiling temperature of the water. The proposed geometry possesses axial symmetry which will reduce the computational cost of solving the system. The system fields arise from the impressed current density which models the coil. The upper medium is a ferromagnetic and conductive material, i.e., the system load, which is replaced by the nonlinear IBC, and the lower material is a perfect magnetic material whose purpose is to increase the magnetic coupling between the coil and the system load. The preceding structure corresponds to a simple induction heating, IH system characterized by its equivalent coil impedance, Z_{coil}, [41], [42].

TABLE I: Geometry of the reference eddy current system.

Parameter	value
Coils internal radius	10 mm
Coils external radius	30 mm
Coil's tickness	4 mm
Coil number of turns	48
Coil-load distance	4 mm
Coil-ferrite distance	1 mm

The geometrical parameters of the reference IH system are listed in Table I. The current amplitude I_{coil} driven by each turn of the coil is associated with the current $i(t) = \text{Re}\left(I_{\text{coil}} e^{j\omega t}\right)$, therefore, the coil is modeled as a uniform impressed current density of value $J_{\text{coil},\varphi} = \frac{nI_{\text{coil}}}{S_{\text{coil}}}$, where the cross-sectional area is equal to $S_{\text{coil}} = (r_{\text{ext}} - r_{\text{int}})\, t$. On the one hand, the coil is placed at the distance $d_f = 1$ mm above the ferrite medium characterized by an extremely high magnetic permeability modeled by the boundary condition of perfect magnetic material. On the other hand, the coil is located at $d_l = 4$ mm below the load material. Solving of fields involved in the system will be performed in a commercial tool, in this case, COMSOL®, due to the numerical model of the IH system can be constructed in a simple way and incorporates the possibility of using an impedance boundary condition dependent on the excitation level. The schematic representation of the geometry is shown in Fig. 7: coil is drawn in purple, load, air, and ferrite are colored in orange, yellow, and grey, respectively. Linear IBC is included in the COMSOL

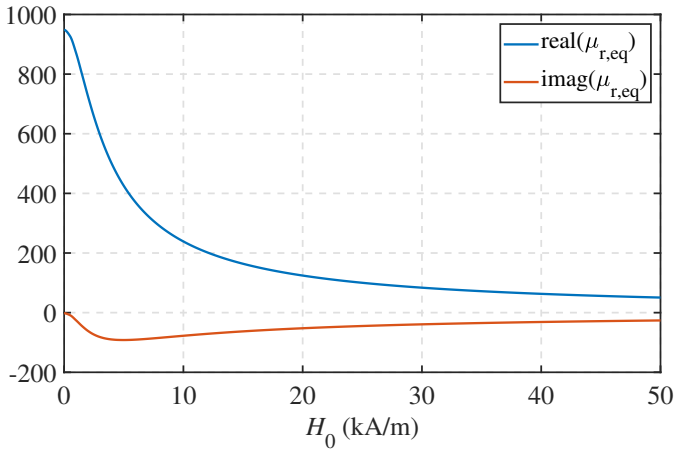

Fig. 8: Reference equivalent relative permeability $\mu'_{\text{r,eq}}$ for $a_0 = 560$ A/m and $B_{\text{sat},0} = 2$ T.

model providing the relative permeability and conductivity of the load. The nonlinear IBC can similarly be included by defining the equivalent relative permeability at each excitation level H_0, as follows:

$$\mu_{\text{r,eq}}(H_0) = \frac{2\sigma}{\omega\mu_0}\left(\frac{Z_{\text{NL}}(H_0)}{1+j}\right)^2. \tag{43}$$

The real and imaginary components of the reference relative permeability $\mu'_{\text{r,eq}}(H'_0)$ for $a_0 = 560$ A/m and $B_{\text{sat},0} = 2$ T calculated at $f_0 = 10$kHz and $\sigma_0 = 1.12{\cdot}10^7$ S/m by applying (43) are depicted in Figure 8. The FEA tool internally obtains the equivalent permeability for the corresponding configuration by applying the following expression derived from (42) and (43) :

$$\mu_{\text{r,eq}}(H_0) = \frac{B_{\text{sat}}}{B_{\text{sat},0}}\frac{a_0}{a}\mu'_{\text{r,eq}}\left(H_0\frac{a_0}{a}\right), \tag{44}$$

Therefore, the reference permeability only needs to be calculated on one occurrence and the corresponding permeability is derived for each configuration internally by the FEA tool.

The induced voltage in the coil can be obtained in a simple way from the solution of the fields, according to the expression $V_{\text{coil}} = -n\langle 2\pi r E_\varphi\rangle_{S_{\text{coil}}}$ where r is the radial distance to the axis of the system reference, $E_\varphi$is the electric field carried out from the simulation and $\langle\rangle_{S_{\text{coil}}}$ is the spatial mean operator in the cross-section area of the coil. The key figure of merit of the IH system is the complex coil impedance $Z_{\text{coil}} = V_{\text{coil}}/I_{\text{coil}}$. The induced voltage in a non-loaded coil is in quadrature with respect to the coil current, therefore, at any frequency, the phase of the coil impedance is 90°. However, the insertion of linear magnetic and conductive media near the coil produce a frequency dependence of the phase of the coil impedance, but the coil impedance remains unchanged under the current level variation.

The coil impedance, Z_{coil}, is calculated from frequency-domain simulations by using $Z_{\text{NL}}(H_0)$ to model the load. The performance assessment of the proposed nonlinear impedance boundary condition will be given by comparison with results obtained by time-domain simulation. In the first place, the

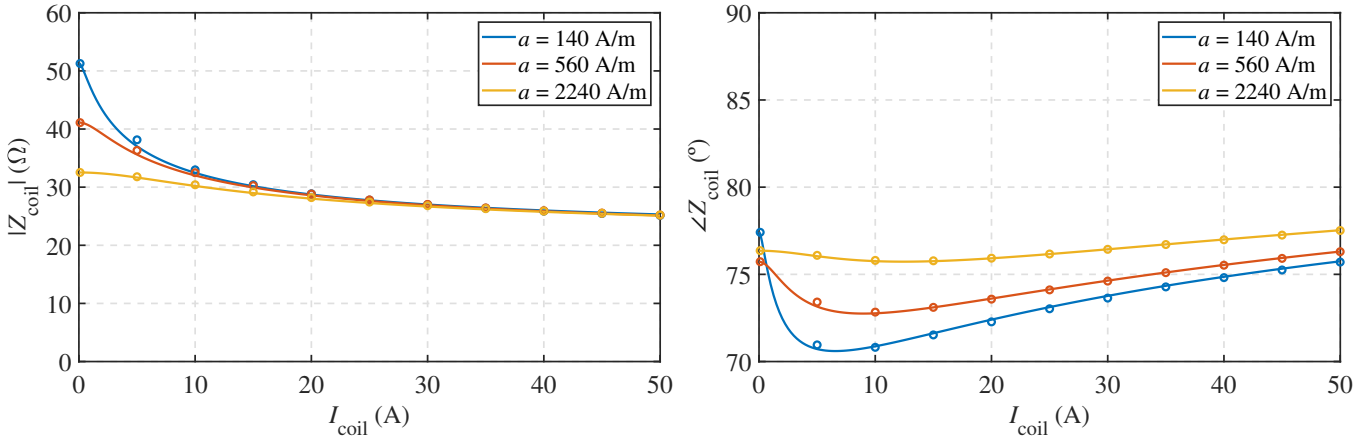

(a) Amplitude of the coil's impedance, $|Z_{\mathrm{coil}}|$.

(b) Phase of the coil's impedance, $\angle Z_{\mathrm{coil}}$.

Fig. 9: First harmonic impedance IH system with respect to the excitation current at $f = 50$ kHz for a load of material with $\sigma = 1.12 \cdot 10^7$ S/m and $B_{\mathrm{sat}} = 2$ T, varying a (continuous lines: data using Z_{NL}; circular symbols: first harmonic extraction from time domain simulation).

system fields will be solved using a time-domain simulation with a Langevin function BH-loop load. From the time dependence of the induced voltage, the first harmonic of the coil voltage $V_{\mathrm{coil},1}$ is extracted and the coil impedance is derived from the ratio to the current amplitude $Z_{\mathrm{coil},1} = V_{\mathrm{coil},1}/I_{\mathrm{coil}}$. The main drawback of the time-domain simulation is the requirement of very fine meshing in the load surface, where exponential discretization is recommended due to the rapid variation of the fields. On the contrary, simulation utilizing the nonlinear IBC Z_{NL} constitutes a cost-effective solution because no discretization is required for the load, thus, high computational savings are achieved with this approach.

Fig. 9 shows the comparison between the coil impedance calculated using the nonlinear boundary condition modeling the load and the first harmonic coil impedance carried out from time domain simulation. The data depicted in these figures corresponds to the variation of the domain wall parameter a, with constant frequency, load conductivity, and saturation magnetic field. It can be seen the agreement between the values of the coil impedance, both amplitude and complex phase, are quite good considering the approximation taken in the derivation process. Time-domain results also include higher harmonic contributions closely related to the saturation of the material. In any case, the influence of the distortion in the first harmonic contribution is almost totally included in the nonlinear IBC estimation.

In Fig. 10 is compared the coil impedance from nonlinear IBC and time domain first harmonic extraction for different magnetic field saturation of the material. Based on the data presented in Fig. 10a, it is evident that the absolute value of the coil impedance is significantly influenced by the degree of saturation in the material. Therefore, in induction heating systems, the saturation level of the material utilized plays a crucial role in determining the coil impedance. Moreover, as depicted in Fig. 10b, the complex phase of the coil impedance also clearly depends on the saturation magnetization of the material. Fig. 10 shows a good agreement between the results obtained from the nonlinear boundary condition, validating the usefulness of this kind of approach to the treatment of eddy current problems where saturation plays an important role.

V. Conclusion

In certain problems related to electromagnetism, the fields exhibit a rapid decay as they penetrate into specific media. In such cases, it is advantageous to replace the regions with rapidly varying fields with a boundary impedance condition, which simplifies the problem. This approach is effective when the equations governing the rapidly varying field behavior are linear. However, the saturation phenomenon can lead to the appearance of non-harmonic distortion, which might render this approach unsuitable.

The Langevin function BH-loop holds significant physical significance in modeling the saturation of magnetic properties in materials through the anhysteretic Jiles-Atherton model. The finite difference method has been implemented to obtain the nonlinear boundary impedance, which balances accuracy and complexity, for the preceding magnetic properties dependence. The value of the nonlinear boundary impedance is reliant on the applied excitation level. Despite the seemingly vast number of degrees of freedom to describe the characteristics of a medium with saturation, the nonlinear boundary impedance values can be obtained from a single curve by applying appropriate normalization. Validation of the normalized expression of the nonlinear boundary impedance has been conducted through comparison with simulation results in the time domain.

The implementation of a nonlinear boundary condition for electromagnetic systems has the potential to deliver noteworthy savings in computational costs. This is due to its ability to facilitate simulations in the frequency domain, which are capable of capturing the nonlinear behavior of a load that has saturated magnetic properties. This approach can offer a significant advantage in terms of more efficient and accurate modeling of complex electromagnetic systems.

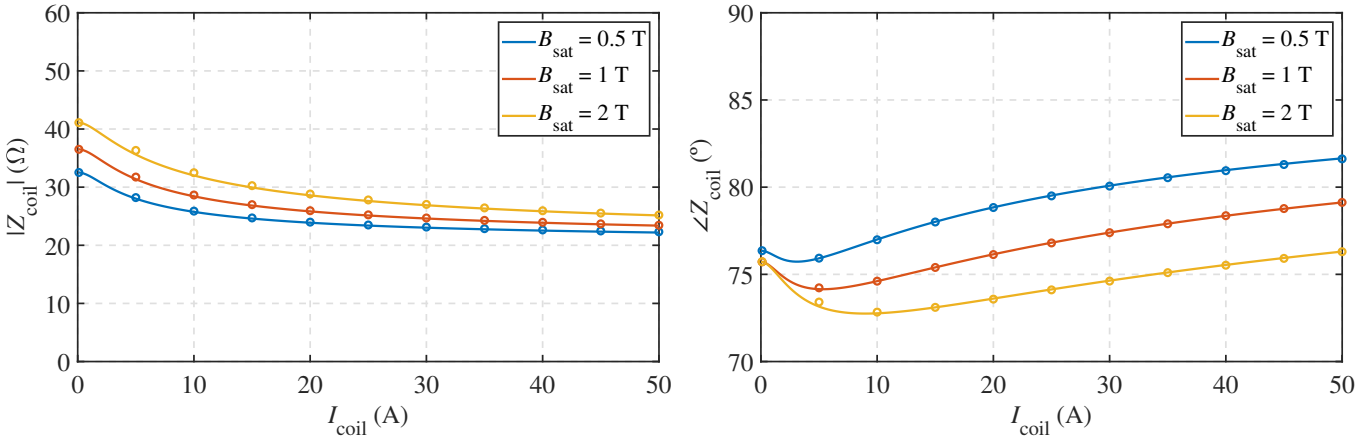

(a) Amplitude of the coil's impedance, $|Z_{\mathrm{coil}}|$.

(b) Phase of the coil's impedance, $\angle Z_{\mathrm{coil}}$.

Fig. 10: First harmonic impedance IH system with respect to the excitation current at $f = 50$ kHz for a load of material with $\sigma = 1.12 \cdot 10^7$ S/m and domain wall parameter $a = 560$ A/m, varying B_{sat} (continuous line: data using Z_{NL}; circular symbols: first harmonic extraction from time domain simulation).

ACKNOWLEDGEMENT

This work was partly supported by the Spanish MCIN/AEI/10.13039/501100011033 under Project PID2019-103939RB-I00, Project PDC2021-120898-I00, Project TED2021-129274B-I00, Project CPP2021-008938, Project ISCIII PI21/00440 and Project PID2022-136621OB-I00, co-funded and by EU through FEDER and NextGenerationEU/PRTR programs, by the DGA-FSE, and by the BSH Home Appliances Group.

REFERENCES

[1] S. Lupi, "Planar circular coils for induction heating," *Electrowarme International*, vol. 37, pp. 319–326, 1979.

[2] C. Carretero, J. Acero, R. Alonso, J. M. Burdío, and F. Monterde, "Modeling mutual impedances of loaded non-coaxial inductors for induction heating applications," *IEEE Transactions on Magnetics*, vol. 44, no. 11 PART 2, pp. 4115–4118, 2008.

[3] J. Acero, C. Carretero, R. Alonso, and J. M. Burdio, "Quantitative evaluation of induction efficiency in domestic induction heating applications," *IEEE Transactions on Magnetics*, vol. 49, no. 4, pp. 1382–1389, 2013.

[4] T. A. Jankowski, N. H. Pawley, L. M. Gonzales, C. A. Ross, and J. D. Jurney, "Approximate analytical solution for induction heating of solid cylinders," *Applied Mathematical Modelling*, vol. 40, no. 4, pp. 2770–2782, 2016.

[5] J. Acero, C. Carretero, I. Lope, R. Alonso, and J. M. Burdío, "Analytical solution of the induced currents in multilayer cylindrical conductors under external electromagnetic sources," *Applied Mathematical Modelling*, vol. 40, no. 23, pp. 10 667–10 678, 2016.

[6] C. V. Dodd and W. E. Deeds, "Analytical solutions to eddy current probe coil problems," *Journal of Applied Physics*, vol. 39, no. 6, pp. 2829–2838, 1968.

[7] X. Yan, S. Dai, and T. Ma, "Electromagnetic and thermal analysis of cylindrical aluminum billet heated by 1 MW HTS DC induction heater," *IEEE Access*, vol. 8, pp. 144 112–144 121, 2020.

[8] K. Kubiczek and M. Kampik, "Fast and numerically stable analytical computations for the power induced in cylindrical multilayered conductors under external magnetic fields," *IEEE Transactions on Electromagnetic Compatibility*, vol. 65, no. 1, pp. 292–299, 2023.

[9] A. Boadi, Y. Tsuchida, T. Todaka, and M. Enokizono, "Designing of suitable construction of high-frequency induction heating coil by using finite-element method," *IEEE Transactions on Magnetics*, vol. 41, no. 10, pp. 4048–4050, 2005.

[10] L. C. Meng, K. W. E. Cheng, and S. L. Ho, "Multicoils design for induction cookers with applying switched exciting method," *IEEE Transactions on Magnetics*, vol. 48, no. 11, pp. 4503–4506, 2012.

[11] R. Naar and F. Bay, "Numerical optimisation for induction heat treatment processes," *Applied Mathematical Modelling*, vol. 37, no. 4, pp. 2074–2085, 2013.

[12] K. Pericleous, V. Bojarevics, G. Djambazov, R. A. Harding, and M. Wickins, "Experimental and numerical study of the cold crucible melting process," *Applied Mathematical Modelling*, vol. 30, no. 11, pp. 1262–1280, 2006.

[13] F. Cajner, B. Smoljan, and D. Landek, "Computer simulation of induction hardening," *Journal of Materials Processing Technology*, vol. 157-158, no. SPEC. ISS., pp. 55–60, 2004.

[14] C. Carretero, J. Acero, R. Alonso, and J. M. Burdio, "Normal-mode decomposition of surface power distribution in multiple-coil induction heating systems," *IEEE Transactions on Magnetics*, vol. 52, no. 2, pp. 1–8, 2016.

[15] G. Zhu, X. Liu, L. Li, and J. Zhu, "A novel nonlinearity marginalization technique for effective solution of induction heating problems by cell method," *Journal of Physics D: Applied Physics*, vol. 53, no. 24, p. 245502, 2020.

[16] M. Fisk, M. Ristinmaa, A. Hultkrantz, and L.-E. Lindgren, "Coupled electromagnetic-thermal solution strategy for induction heating of ferromagnetic materials," *Applied Mathematical Modelling*, vol. 111, pp. 818–835, 2022. [Online]. Available: https://www.sciencedirect.com/science/article/pii/S0307904X22003298

[17] M. Gendron, B. Hazel, E. Boudreault, H. Champliaud, and X.-T. Pham, "Coupled thermo-electromagnetic model of a new robotic high-frequency local induction heat treatment system for large steel components," *Applied Thermal Engineering*, vol. 150, pp. 372–385, 2019.

[18] T. Senior, "Impedance boundary conditions for imperfectly conducting surfaces," *Applied Scientific Research, Section B*, vol. 8, no. 1, pp. 418–436, 1960.

[19] S. Yuferev and N. Ida, *Surface Impedance Boundary Conditions. A Comprehensive Approach*, 1st ed. Boca Raton: CRC Press, 2009.

[20] J. Dong and L. Di Rienzo, "FEM and BEM implementations of a high order surface impedance boundary condition for three-dimensional eddy current problems," *IEEE Access*, vol. 8, pp. 186 496–186 504, 2020.

[21] S. Yin, L. Di Rienzo, X. Ma, and Y. Huangfu, "Boundary Element Formulation Enforcing High-order Surface Impedance Boundary Conditions for Axisymmetric Eddy Current Problems," *IEEE Transactions on Magnetics*, vol. 02, no. c, pp. 1–1, 2021.

[22] A. Canova, F. Dughiero, F. Fasolo, M. Forzan, F. Freschi, L. Giaccone, and M. Repetto, "Simplified approach for 3-D nonlinear induction heating problems," *IEEE Transactions on Magnetics*, vol. 45, no. 3, pp. 1855–1858, 2009.

[23] ——, "Identification of equivalent material properties for 3-D numerical modeling of induction heating of ferromagnetic workpieces," *IEEE Transactions on Magnetics*, vol. 45, no. 3, pp. 1851–1854, 2009.

[24] W. MacLean, "Theory of strong electromagnetic waves in massive Iron," *Journal of Applied Physics*, vol. 25, p. 1267, 1954.

[25] P. D. Agarwal, "Eddy-current losses in solid and laminated iron," *Transactions of the American Institute of Electrical Engineers, Part I: Communication and Electronics*, vol. 78, no. 2, pp. 169–181, 1959.
[26] E. M. Deeley and B. J. Chalmers, "Surface impedance of saturating iron in travelling fields," *IEE Proceedings A - Physical Science, Measurement and Instrumentation, Management and Education - Reviews*, vol. 132, no. 4, pp. 171–177, 1985.
[27] R. Escarela-Perez, S. Maximov, J. C. Olivares-Galvan, E. Melgoza, and M. A. Arjona, "Effective nonlinear surface impedance of conductive magnetic slabs," *IEEE Transactions on Magnetics*, vol. 53, no. 5, pp. 1–12, 2017.
[28] M. Jufer and A. Apostolides, "An analysis of eddy current and hysteresis losses in solid iron based upon simulation of saturation and hysteresis characteristics," *IEEE Transactions on Power Apparatus and Systems*, vol. 95, no. 6, pp. 1786–1794, 1976.
[29] V. Cirimele, F. Freschi, L. Giaccone, and M. Repetto, "Finite formulation of surface impedance boundary conditions," *IEEE Transactions on Magnetics*, vol. 52, no. 3, pp. 1–4, 2016.
[30] F. Azzouz and M. Feliachi, "Non-linear surface impedance taking account of thermal effect," *IEEE Transactions on Magnetics*, vol. 37, no. 5, pp. 3175–3177, 2001.
[31] C. Guerin, G. Meunier, and G. Tanneau, "Surface impedance for 3D nonlinear eddy current problems-application to loss computation in transformers," *IEEE Transactions on Magnetics*, vol. 32, no. 3, pp. 808–811, 1996.
[32] W. Mai and G. Henneberger, "Field and temperature calculations in transverse flux inductive heating devices heating nonparamagnetic materials using surface impedance formulations for nonlinear eddy-current problems," *IEEE Transactions on Magnetics*, vol. 35, no. 3, pp. 1590–1593, 1999.
[33] R. M. D. Vecchio and R. Ahuja, "Analytic nonlinear correction to the impedance boundary condition," *IEEE Transactions on Magnetics*, vol. 49, no. 12, pp. 5687–5691, 2013.
[34] J. Nerg and J. Partanen, "A simplified FEM based calculation model for 3-D induction heating problems using surface impedance formulations," *IEEE Transactions on Magnetics*, vol. 37, no. 5, pp. 3719–3722, 2001.
[35] F. Freschi, L. Giaccone, and M. Repetto, "Algebraic formulation of nonlinear surface impedance boundary condition coupled with BEM for unstructured meshes," *Engineering Analysis with Boundary Elements*, vol. 88, pp. 104–114, 2018.
[36] A. Canova, F. Freschi, L. Giaccone, and M. Repetto, "Improved efficiency and accuracy using duality in hybrid SIBC-BEM formulation," in *2019 International Applied Computational Electromagnetics Society Symposium (ACES)*, 2019, pp. 1–2.
[37] L. Codecasa, P. Alotto, and F. Moro, "Fast solution of induction heating problems by structure-preserving nonlinear model order reduction," *IEEE Transactions on Magnetics*, vol. 52, no. 3, 2016.
[38] T. Fawzi, M. Ahmed, and P. Burke, "On the use of the impedance boundary conditions in eddy current problems," *IEEE Transactions on Magnetics*, vol. 21, no. 5, pp. 1835–1840, 1985.
[39] J. Füzi, "Eddy currents in ferromagnetic sheets taking magnetic hysteresis nonlinearities into account," *Periodica Polytechnica Electrical Engineering*, vol. 39, no. 2, pp. 131–143, 1995.
[40] D. C. Jiles and D. L. Atherton, "Theory of ferromagnetic hysteresis," *Journal of Magnetism and Magnetic Materials*, vol. 61, no. 1-2, pp. 48–60, 1986.
[41] J. Serrano, I. Lope, J. Acero, C. Carretero, J. M. Burdio, and R. Alonso, "Design and optimization of small inductors on extra-thin PCB for flexible cooking surfaces," *IEEE Transactions on Industry Applications*, vol. 53, no. 1, pp. 371–379, 2017.
[42] I. Lope, J. Acero, and C. Carretero, "Analysis and optimization of the efficiency of induction heating applications with litz-wire planar and solenoidal coils," *IEEE Transactions on Power Electronics*, vol. 31, no. 7, pp. 5089–5101, 2016.